CHARACTERIZING ICE-MAGMA FEATURES IN THE CENTRAL OREGON CASCADES

by

ANA MERCEDES COLÓN UMPIERRE

A THESIS

Presented to the Department of Earth Sciences
and the Division of Graduate Studies of the University of Oregon
in partial fulfillment of the requirements
for the degree of
Master of Science

December 2021

THESIS APPROVAL PAGE

Student: Ana Mercedes Colón Umpierre

Title: Characterizing Ice-Magma Features in the Central Oregon Cascades

This thesis has been accepted and approved in partial fulfillment of the requirements for the Master of Science degree in the Department of Earth Sciences by:

Meredith Townsend	Chairperson
Thomas Giachetti	Member
Doug Toumey	Member

and

Krista Chronister	Vice Provost for Graduate Studies

Original approval signatures are on file with the University of Oregon Division of Graduate Studies.

Degree awarded December 2021

THESIS ABSTRACT

Ana Mercedes Colón Umpierre

Master of Science

Department of Earth Sciences

December 2021

Title: Characterizing Ice-Magma Features in the Central Oregon Cascades

Hogg Rock is a basaltic-andesite dome located in the Central Oregon Cascades. Its flat top, steep sides, and glacial striations and lakes have led to the interpretation that Hogg Rock was a dome that erupted subglacially. It is also highly fractured, a characteristic often found in ice-magma deposits. We mapped the fractures at Hogg Rock and found three different types of fractures: cube joints, plate joints (also known as entablature), and pseudo-columnar joints. We also mapped the orientations of the fractures where possible. We found that the fractures were mainly horizontal and radially oriented around the butte, suggesting that Hogg Rock cooled from the outside in, and further supporting the interpretation that Hogg Rock erupted subglacially. We also measured the fracture density of the joints, and found that the platey joints represented the finest scale of jointing.

CURRICULUM VITAE

NAME OF AUTHOR: Ana Mercedes Colón Umpierre

GRADUATE AND UNDERGRADUATE SCHOOLS ATTENDED:

University of Oregon, Eugene

Dartmouth College, Hanover

DEGREES AWARDED:

Master of Science, Earth Sciences, 2021, University of Oregon

Bachelor of Arts, Earth Sciences and Astronomy, 2018, Dartmouth College

AREAS OF SPECIAL INTEREST:

Geology

Natural Hazards

PROFESSIONAL EXPERIENCE:

Graduate Employee, University of Oregon, 2019-2021

Interpretive Park Ranger, National Park Service, 2018-2019

El Morro National Monument, Ramah, NM

GRANTS, AWARDS, AND HONORS:

Student Research Grant, Central Oregon Geoscience Society, 2021

Honorable Mention, NSF Gradate Research Fellowship Program, 2021

Promising Scholar Award, University of Oregon, 2019

Mellon Mays Undergraduate Fellowship, Dartmouth College, 2016

ACKNOWLEDGMENTS

I would like to thank my advisor, Meredith Townsend, for her financial support and mentorship throughout this degree. Those wishing to access drone data alluded to in this thesis may contact her at mtownse4@uoregon.edu. I would also like to thank my other committee members, Thomas Giachetti, Doug Toumey, and Leif Karlstrom, for continual mentorship in graduate school. Additionally, I would like to thank the Central Oregon Geoscience Society for their financial support of my project. I also want to thank the 2021 Earth Sciences Field Camp group, for allowing me to treat them like an army of data collection robots for my project - you are all wonderful people, and I look forward to seeing what you get up to in the future.

Un millón de gracias to my closest friends. Thank you to David for being the best roommate a gal could ask for, providing me with perspective, a reality check when needed, and a continuous supply of tasty drinks and candy for morale. Thank you to PJ for constant entertainment and encouragement when I so direly needed it in the office (and outside the office). Thank you also for all the rides to school. Thank you to Gen for being the most understanding person I have ever met, and being on the same wavelength when it mattered the most. Thank you to Helen and Diego and Will Tackett for being the strongest support system, even when many miles and time zones apart, I miss you guys every day. Thank you to Aydin for understanding me on the deepest level, and knowing exactly what to say when I need to hear it. Los amo amo amo a todos, y sin ustedes seguramente estaría en limbo por siempre. Finally, thank you to Ceiba and Fen for being cute.

This thesis is dedicated to my dog Ceiba and her best friend Fen.

TABLE OF CONTENTS

LIST OF FIGURES

Figure Page

Figure Page

CHAPTER I: INTRODUCTION AND BACKGROUND

Glaciovolcanism: Why study it?

Glaciovolcanism refers to the interaction between magma and ice in all its forms, including glaciers, snow, glacial melt, etc. Volcanic systems in general are some of the most destructive natural hazards that affect society on human timescales. Ice-covered volcanoes in particular pose additional hazards unique to glaciated systems, such as massive meltwater flooding (known as jökulhlaups), and enhanced tephra production. A recent notable example of a destructive glaciovolcanic eruption is Eyjafjallajökull in 2010. Although a relatively small eruption, this event shut down air travel across Europe and cost the airline industry $1.7 billion. The increased hazards associated with magma-ice interaction make monitoring glaciated volcanoes crucial to minimizing damage to life, infrastructure, and the economy.

Monitoring glaciated systems proves to be a challenge. The signs of volcanic unrest at a glaciated volcano are inherently different from those in non-glaciated systems. For example, eruptions in glaciated systems tend to produce ice cauldrons, areas of widespread subsidence caused by the sudden discharge of ice melt at the base of the glacier, punctures in the ice carved out by steam, and deposition from debris flows (for example, see Bleick et al. (2013) for an excellent summary of ice deformation features leading to the eruption of the glaciated volcano Redoubt in 2009). While this study does not focus on ice cauldrons, there is a growing body of literature on their use in hazard assessment (see Evatt & Fowler (2007), Magnús T. Gudmundsson (2003), Oddsson et al., (2016) and Reynolds et al. (2017) for studies on ice cauldrons and their relations to subglacial volcanic activity). Traditional volcano monitoring tools, such as satellite-based measurements of surface deformation and models relating surface deformation to underlying magmatic processes, are not sufficient for characterizing unrest underneath ice. The challenge is

that the mechanics of magma-ice interaction at the bottom of glaciers during an eruption are still not well understood. Wilson & Head (2007) propose simplified thermal models for different mechanisms of magma emplacement within ice at the ground/ice interface, but they do not directly relate observables like meltwater discharge or ice deformation to the underlying style of eruption. Some recent work by Gudmundsson et al. (2004) attempts to more directly link ice cauldron formation to the volumes of magma emplaced under ice. However, models for magma-ice interaction have yet to be tested against direct field observations.

Magma-ice deposits from past eruptions that are now exposed can provide constraints on how magma interacts with glacial ice and water. In addition, these deposits can provide information about local paleo-ice conditions. Dating these deposits can provide constraints on the time when ice was present locally. Certain lithological features of magma-ice deposits can provide even more details about the size and structure of ice present at the time of eruption. For example, "passage zones" are the layer of tuyas (volcanoes that erupt underneath glaciers) characterized by a depositional surface separating subaqueous from subaerial deposits, both effusive and explosive. The interpretation of these boundaries is that they mark where the eruption transitioned from beneath the glacial level and partially under glacial melt, to above the glacial level and erupting subaerially. Variations in the elevation of a passage zone can record changes in the level of glacial lakes controlled by glacial hydrology, or subglacial drainage (Edwards et al., 2015). In other words, these can provide information on glacial morphology and geometry at a specific point in time (see Russell et al. (2014) section 4.4 *Tuyas as paleoclimate proxies*) for more information on the topic).

Glaciovolcanism: What we know

Ice-magma deposits are widespread, and glaciovolcanic eruptions have been documented in Antarctica, Iceland, British Columbia, and the Pacific Coast of North and South America, among others (Smellie & Edwards, 2016). Field-based studies have identified several of the key lithologic and structural features that are characteristic to magma-ice deposits. The key to identifying an ice-magma deposit is to find evidence of confinement and evidence for the presence of water (Edwards et al., 2015). The characteristics of volcanic rocks deposited in ice-dominated environments are described as follows (adapted from Edwards et al. (2015)):

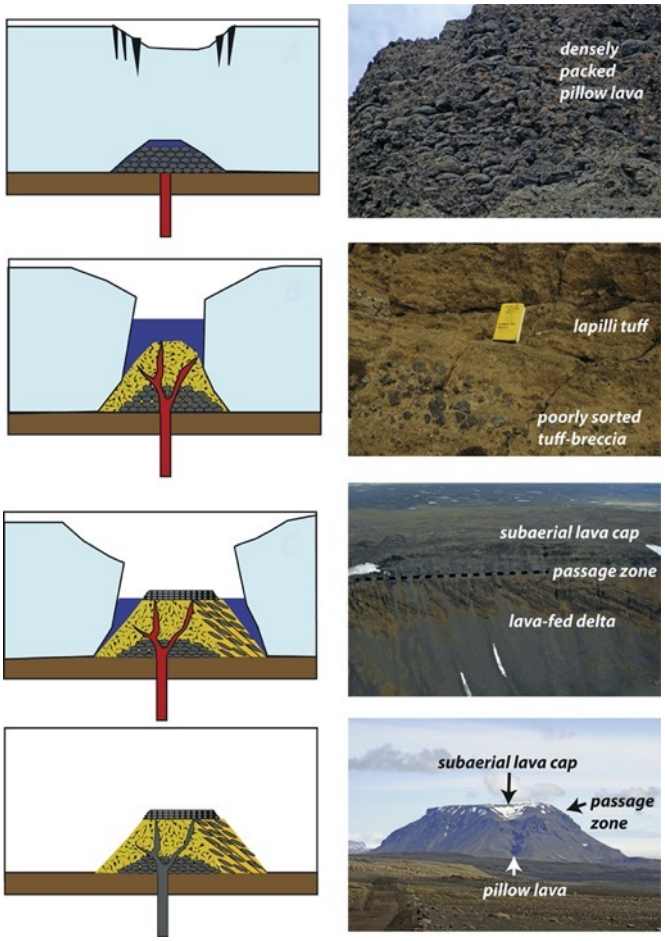

Figure 1: Schematic of the four stages of the classic tuya model, with images of the resulting deposits. Adapted from Edwards et al. (2015)

1) Deposits recording the effects of ice confinement, such as vertical cooling surfaces, thermal fractures, steep beds, anomalously thick lava flows, and pervasive palagonite suggesting retention of heat in a water-rich environment.
2) Deposits recording the effects of rapid cooling, such as thermal fractures (columnar joints, cooling columns) with anomalously small widths and anomalous orientations, pillow lavas interbedded with hyaloclastite (volcanoclastic deposits formed by explosive magma-water

interactions (McGarvie, 2009)), and volcanoclastic deposits dominated by vitric (glassy) particles

3) Deposits recording multiple fragmentation processes, such as fine ash, poor sorting, block sized fragments
4) Deposits recording subaqueous/subaerial transitions

Most of these characteristics are based on current publications of field measurements of ice-magma deposits, which disproportionately have been conducted on basaltic deposits. Observations of these basaltic deposits have led to the creation of "The Classic Model" for a glaciovolcanic eruption, and the lithofacies these leave behind. The classic model of a tuya-forming eruption is broken down into four stages, each comprising a distinct layer of the final deposit. During the first stage of the eruption, a dike erupts effusively at the base of the ice, with ice thicknesses assumed to be thick enough to restrict explosivity. The main effusive product in this stage is pillow lava, with minor hyaloclastites. During stage 2, the eruption switches from mainly effusive (creating coherent deposits) to mainly fragmental. This change is linked to the growing mound of pillows leading to a decreased water pressure (from the increasing height of the edifice within the formed meltwater glacial lake, and the deformation and subsidence of ice above it creating an ice cauldron). This ice subsidence allows for the ice load to be supported by the surrounding ice, reducing the pressure and leading to increased explosive phreatomagmatic activity. During stage 3, the bulk of the edifice has breached the surface, so the lava moves laterally away from the edifice towards the edge of the lake and builds a lava delta. This creates a boundary between subaqueous and subaerial eruption products (the passage zone). Finally, stage 4 is when the glacier melts on glacial timescales (not due to the eruption), and reveals a flat-topped, steep sided basaltic volcanic deposit.

While most descriptions of glaciovolcanic deposits are from basaltic deposits, recent advances in field-based studies of intermediate to silicic glaciovolcanism show that intermediate composition lavas do not always follow the "classic model," but show less fragmental material than basaltic lavas, and that deposit morphology and cooling joints are key to recognition of their glaciovolcanic origin (McGarvie, 2009). However, very little work has been done to make detailed and crucial descriptions of these features to relate them directly to thermal history and magma-ice interaction processes (see Forbes et al. (2014) for descriptions of different fracture types). More detailed descriptions and quantitative data would provide some insight on not only key characteristics of these more intermediate deposits, but also on how these deposits form in the first place.

Furthermore, most of the studies that describe intermediate and silicic tuyas were conducted in Iceland (see Farquharson et al. (2015) and Tuffen & Castro (2009)), and there is a paucity of studies on intermediate glaciovolcanic deposits from subduction zones, despite their prevalence in these settings (such as in Alaska, British Columbia, the Western US, among others). See Allen et al. (1982), Báez. et al. (2002), Báez et al. (2020), Edwards et al. (2011), M. T. Gudmundsson et al. (2002), Lachowycz et al. (2015), Stevenson et al. (2011), among others, for examples of studies of glaciovolcanic features that are intermediate to felsic in composition. While some of these record the presence of columnar joints, there has not been extensive work done on the nature of columns in subglacial eruptions of this composition.

The focus of this thesis is on the fractures formed by rapid cooling in intermediate subglacial eruptions. In particular, the objective is to learn about characteristics of intermediate effusive tuyas with a focus on cooling joints. To do this, I conducted field work at Hogg Rock, which is interpreted as an intermediate subglacial dome, located in the Oregon Cascades. Hogg

Rock is notable due to its extremely fractured nature, making it an ideal place to study the relationship between the rapid cooling in subglacial eruptions and the resulting fractures. I made detailed descriptions of fractures and the different fracture sets present at Hogg Rock, with quantitative measurements on fracture distribution and orientation spatially around the butte, in order to determine the relations between fracture sets and begin to understand the cooling history of this butte. The goal was to provide more insight and fill the knowledge gap that exists in detailed documentation of fracture characteristics in intermediate glaciovolcanic deposits, in order to work towards how thermal fractures can inform thermal history and emplacement history.

Tectonics, Volcanism, and Hydrology of the Central Oregon Cascades

The Western US is riddled with volcanoes. The Cascade volcanic range extends from Northern California into Southern Canada (Figure 2). This volcanic arc results from the subduction of the Juan de Fuca Plate beneath the North American plate and has been active for around 40 million years. In Oregon, the Cascades are bounded to the west by the Willamette Valley and to the east by the Deschutes Basin. Volcanism in this region has not been continuous in space and time throughout this period, and the Oregon Cascades are commonly divided into the Western Cascades and the High Cascades provinces. These provinces are differentiated both by the age of the volcanism, and by an eastern shift in the location of volcanism.

Figure 2: Regional tectonic setting in the Cascades. The Juan de Fuca Plate subducts into the North American plate, creating a volcanic arc. Red triangles denote the volcanoes in the Cascade Volcanic Arc. Photo from NASA (Public Domain)

The Quaternary volcanoes in the Oregon Cascades have over 1,000 vents within 9,500 km^2 (Hildreth, 2007). Some estimates place the production rate in the central Oregon Cascades between 3 to 6km^3 per linear km of arc per million years during the Quaternary (Sherrod & Smith, 1990) of volcanic product. While glaciers have eroded many of the deposits from the Cascades, mafic activity has continued into post-glacial times, with 290km^3 of magma erupted from the Cascades over the past 15,000 years (see figure 4 for a summary of volcanic eruptions in the Cascades during the past 4,000 years).

The Western Cascades are much older, and they are thought to represent the location of the volcanic arc prior to the rotation of the plate over the location of magma production (Deligne, Natalia I. et al., 2017). The volcanic deposits of the Western Cascades consist of a thick assemblage of mafic lava flows and ash flows, with minor silicic intrusions that range in age from 40 Ma to 5 Ma (Deligne, Natalia I. et al., 2017). Outcrops in the Western Cascades are commonly obscured by classic Pacific Northwest greenery, facilitated by the heavy precipitation in the area. This heavy precipitation takes the form of rain in the Western Cascades and snow in the High Cascades. Because of the permeable nature of volcanic deposits and regional faults allowing for water travel, the Western Cascades reveal interesting and dynamic hydrological phenomena, including disappearing streams, cold and hot springs, and tremendous waterfall features (see figure 3). The volcanic-tectonic-hydrologic interactions on display in the Western Cascades today reflect hydrologic complexities that likely operated at the time of glaciovolcanic processes in the past. For anyone wishing to visit the field site discussed in this thesis, these features also make for a wonderful side trip.

Figure 3 Hydrological phenomena of the Western Cascades. The highly permeable nature of basaltic deposits in the area lead to a plethora of springs (3a, hot springs in the Western Cascades are relatively common, and are due to water traveling along faults through the rock) and waterfalls (Salt Creek Falls, 3b, and Sahalie Falls, 3c). I include these images because I took them, and they are only some of the beautiful landscapes I encountered while working on this degree.

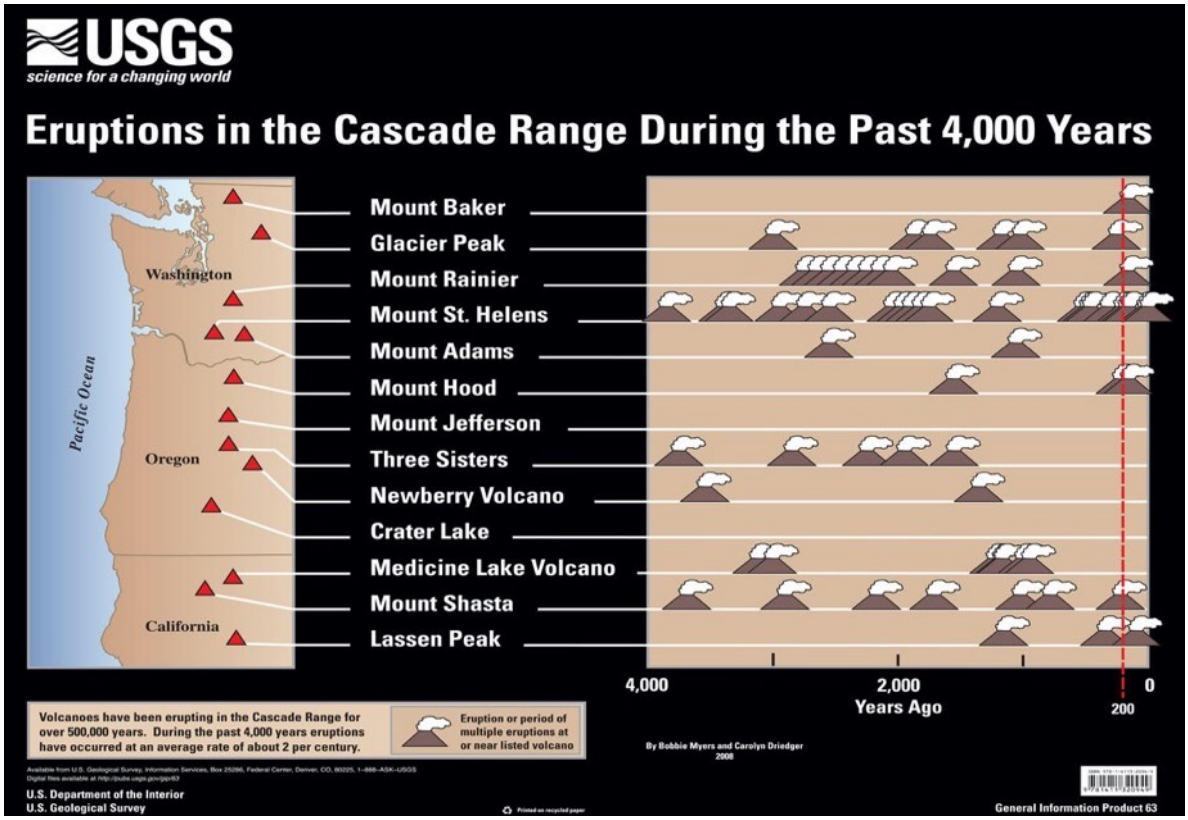

Figure 4: Summary of eruptions in the Cascade Range during the past 4,000 years. Adapted from the USGS.

The effects of snow and ice on volcanic deposits are on clear display today in the modern volcanic arc of the High Cascades. High Cascade stratovolcanoes are constructed on top of 2-3-km-thick lava flows which filled a graben in the older rocks. The stratovolcanoes range from basaltic to rhyolitic in composition, and are composed of interlayered lava flows and pyroclastic deposits, which are revealed in many places where glaciers have carved away parts of the edifice (Figure 5 b,c). In contrast, Mt Bachelor (figure 5d), Middle and South Sister (figure 5e) have well-preserved conical morphology of mafic shield and stratovolcanoes, indicating that their volcanic activity has either outpaced or postdated glacial erosion. In addition to erosional effects, glaciers have also impacted volcanic eruptions in the past, as evidenced by palagonite tuffs in strata at North Sister (Schmidt and Grunder, 2009), tuyas of the Matthieu Lakes Fissure (Schmidt and Grunder, 2009), and the tuyas in Santiam Pass which are the focus here.

Due to the lack of geological constraints, there are few local models of paleoclimate for Oregon. However, with models based on ice cores from Greenland and Antarctica, there are some reconstructions for large scale ice cover in the US around the time Hogg Rock was thought to have erupted. Current age estimates for Hogg Rock place the eruption as having occurred during or soon after the Wisconsin glaciation at about 0.11Ma (Jouzel et al., 1987). In addition to paleoclimate reconstructions, studies have observed and recorded evidence for interaction with ice in volcanic deposits in the Cascades (Lodge & Lescinsky, 2009). Thus, we can assume that glaciers have been present for much of the time that the volcanoes in the Cascades have erupted.

Figure 5: Large Cascade volcanoes on film. 5a) Mt. Rainier, 5b) Broken Top, 5c) Mt Washington from Big Lake, 5d) Mt Bachelor, 5e) South and Middle Sister from the summit of Broken Top

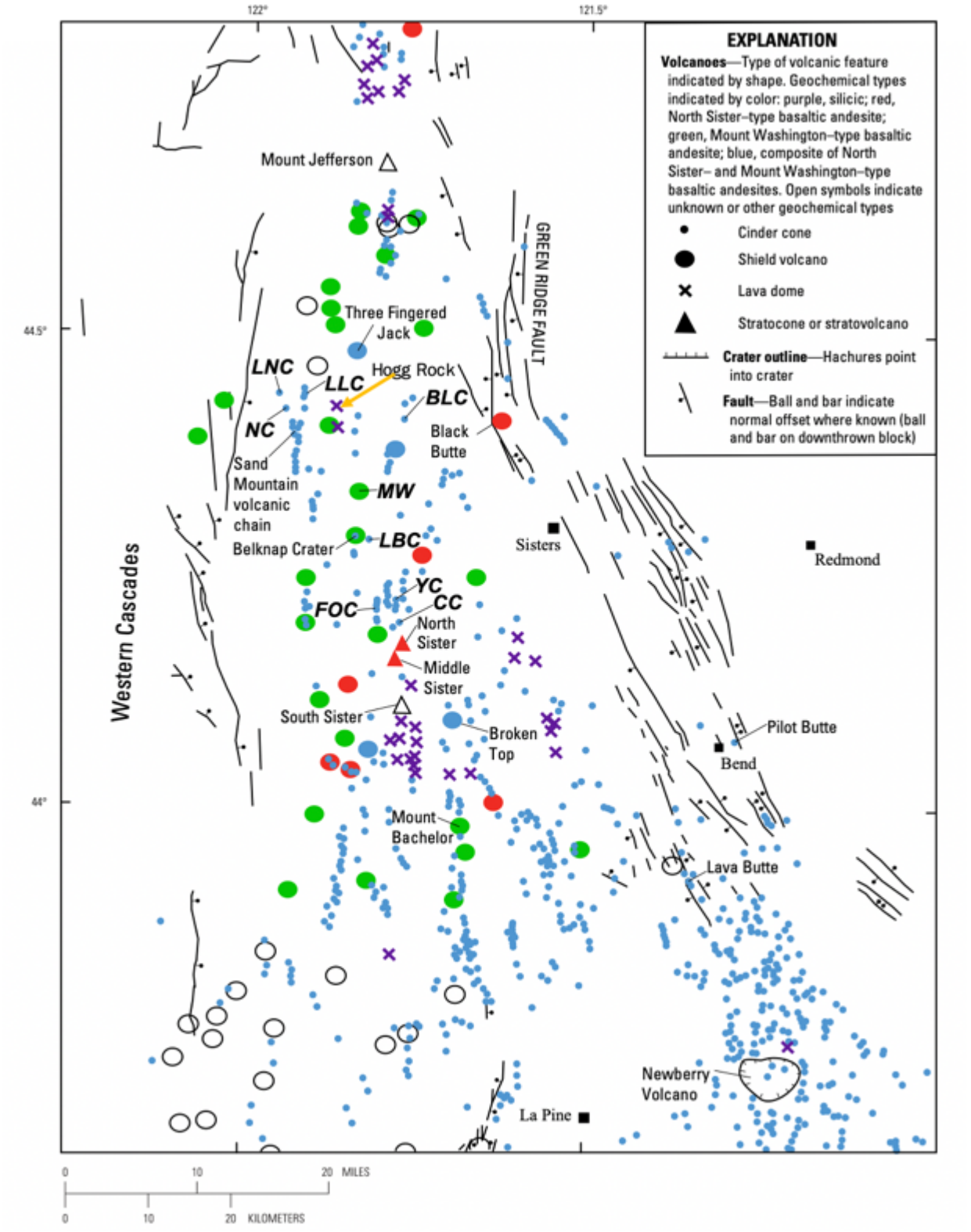

Figure 6: Distribution of faults and Quaternary volcanic vents in the Central Oregon Cascades (adapted from Deligne et al. 2017). Hogg Rock is labeled with a purple X and text label.

CHAPTER II: FIELD SITE

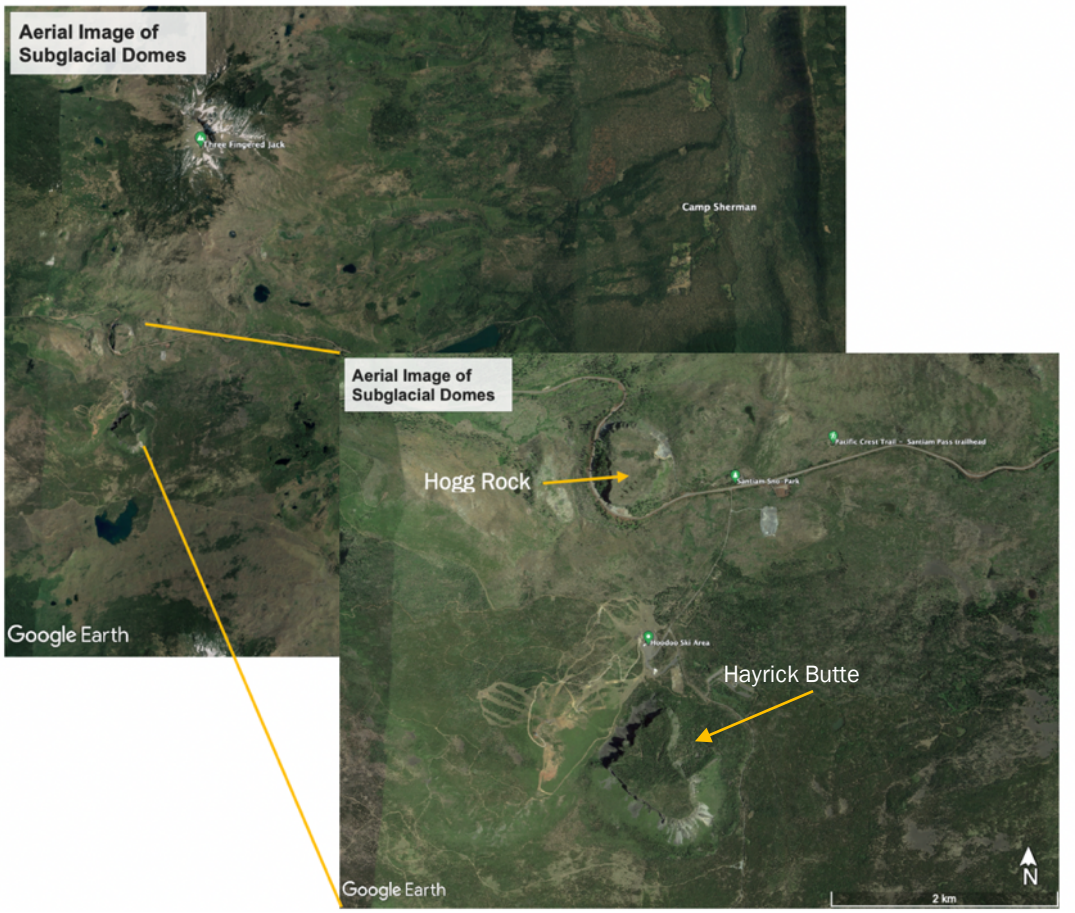

Figure 7: Aerial image of the field site, Hogg Rock. The image on the left is a zoomed out aerial image, showing its position relative to Black Butte and Three Fingered Jack (see Figure 6 for context). The bottom image shows a close up of Hayrick Butte (bottom) and Hogg Rock (top)

The goal of this project is to characterize glaciovolcanic features in the Oregon Cascades. To do this, we focused on Hogg Rock and Hayrick Butte (see Figure 6 and Figure 7 for location), volcanic deposits believed to be subglacial domes. Hogg Rock and Hayrick Butte are aligned along a north-south trend, and it is unclear whether they are separate eruptions or fed from a common fissure. The overall morphology of these features, and their flat tops and steep-cliff sides in particular, are characteristic of subglacial eruptions. Although we made general field observations

at both Hayrick Butte and Hogg Rock, ultimately, we took a more focused approach to study Hogg Rock because of its smaller size and greater accessibility.

Studies of Hogg Rock are limited. A 1992 USGS Report on the geology of Santiam Pass provides a brief description of the butte: "Several small andesitic domes were erupted at Hogg Rock and Hayrick Butte about 4 km west and 6 km southwest of the well site respectively. These andesite domes have steep sides with glassy margins and sub-horizontal columns, relatively flat tops, and are anomalously thick, all of which are features generally ascribed to subglacial eruptions. The tops of these andesitic units have been extensively eroded by glaciation, and it is possible that Hogg Rock and Hayrick Butte are subaerial andesite domes that have been extensively glaciated" (adapted from Hill, 1992). Note, the aforementioned well site is a drilled hole made by the USGS located just east of Hogg Rock on OR-20 (see Hill 1992, Figure 6). A Kr-Ar date for Hogg Rock dates this eruption to 90,000 ± 2,000 years, which is during or immediately after the early Wisconsin glaciation at ~110,000 years ago (Hill, 1992). The extensive glacial erosion that Hill (1992) describes likely refers to aligned striations and elongated glacial lakes that can be observed at the top of Hogg Rock.

In addition, Hogg Rock has an impressive density of cooling fractures that show a variety of styles, spacing, and orientations. Chaotic and finely-spaced fractures are generally thought to be characteristic of glaciovolcanic deposits related to rapid cooling by the introduction of external ice and water; however, to date there are no systematic characterizations of glaciovolcanic fractures or studies that attempt to link in a quantitative way the relationship between the style and density of fracturing to the cooling history. This project aims to characterize the cooling joints present at Hogg Rock, in order to build on our understanding of the emplacement of Hogg Rock and to better understand magma-ice interaction for intermediate lavas more broadly.

Petrology of Hogg Rock

Hogg Rock has been scarcely sampled before by the USGS during studies of the Santiam Pass. These samples showed that Hogg Rock is composed of basaltic andesite typical of late High Cascades basaltic andesite (Hill, 1992). Other studies of Hogg Rock have sampled glassy margins of the butte, and found that these andesites are less mafic than other basaltic andesites in the area (e.g. The Table at Mount Jefferson) (Hughes 1983). Analyses of Hogg Rock andesite shows that Hogg Rock is primarily made up of silicates, with a SiO_2 content of ~60% (Hill, 1992). Around 20% of the minerals were Aluminum Oxides, with a small amount (<10%) of Sodium Oxides, Magnesium Oxides, and Calcium Oxides (Hill, 1992).

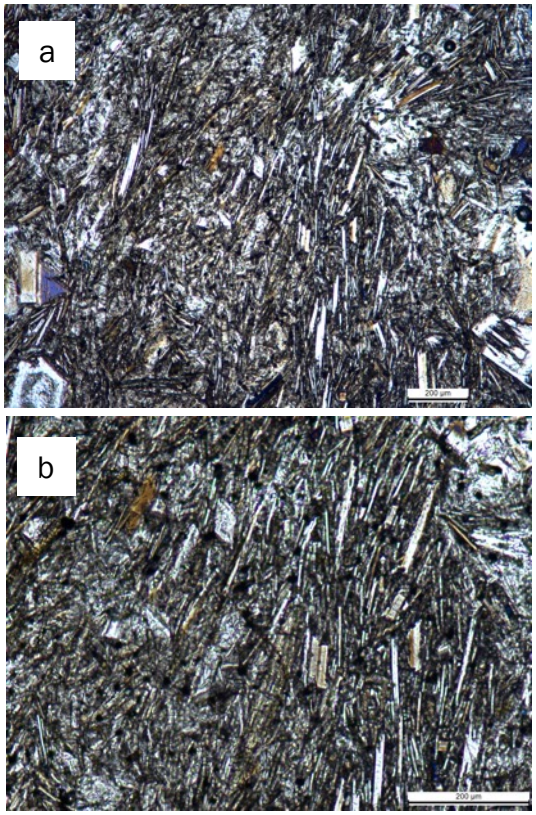

Figure 8: Thin section at 5x magnification (a) and 10x magnification (b) of Hogg Rock.

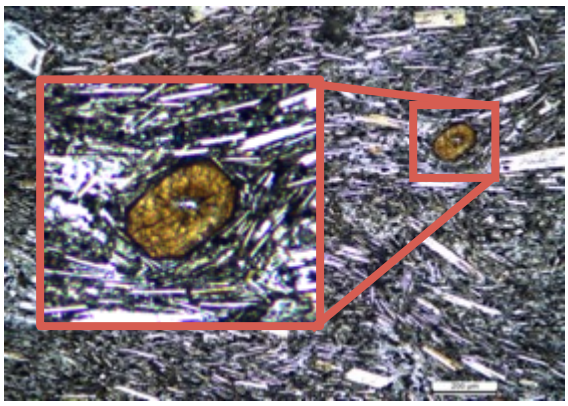
Figure 9: Thin section of Hogg Rock, showing how small crystals seem to align around larger crystals.

In thin section, the texture of the andesites at Hogg Rock is very crystal rich (Figure 17). The bulk of the mineralogy is plagioclase, and the tabular plagioclase minerals demonstrate a strong flow fabric. In some areas, the small plagioclase crystals appear to align around the larger crystals (Figure 18).

CHAPTER III: METHODS

The bulk of the methodology for this project is focused on the fieldwork and descriptions conducted during the summers of 2020 and 2021. First, we made ground-based geologic descriptions of the cooling fractures at Hogg Rock and divided these into three categories based on their morphology (outlined below). After documenting descriptions of the fracture sets, we did a series of fracture mapping for each fracture set encountered. The goal of these measurements was to obtain a fracture density throughout the butte. By providing data on joint density, we can begin to work towards a quantifiable relationship between joint density and thermal cooling history. In addition to these ground-based measurements, we took aerial drone footage to create 3D Structure from Motion modeling in order to map fractures that were inaccessible on foot. Finally, we collected samples for petrographic analysis, and for future work in analyzing the thermal history of Hogg Rock. These, and data from the drone surveys we conducted at Hogg Rock and Hayrick Butte, are available upon request.

Figure 10: The "gravel pit" at Hogg Rock. This is an active quarry, and made for some beautiful exposures of fractures in a deeper cut of the butte.

Cooling Fractures at Hogg Rock

The fractures at Hogg Rock are at first glance chaotic. After careful observation, we split the fractures into three categories: platey joints, cube joints, and pseudo-columnar joints (Figure 9). These characterizations are based off prior work conducted on ice and snow contacts in lava (Forbes et al., 2014; Lodge & Lescinsky, 2009), where they connected the fracture patters to implications for the emplacement of the flow and cooling history (note that this study focused on contact with snow and ice caps after the lava was erupted, rather than for an eruption that occurred underneath the ice).

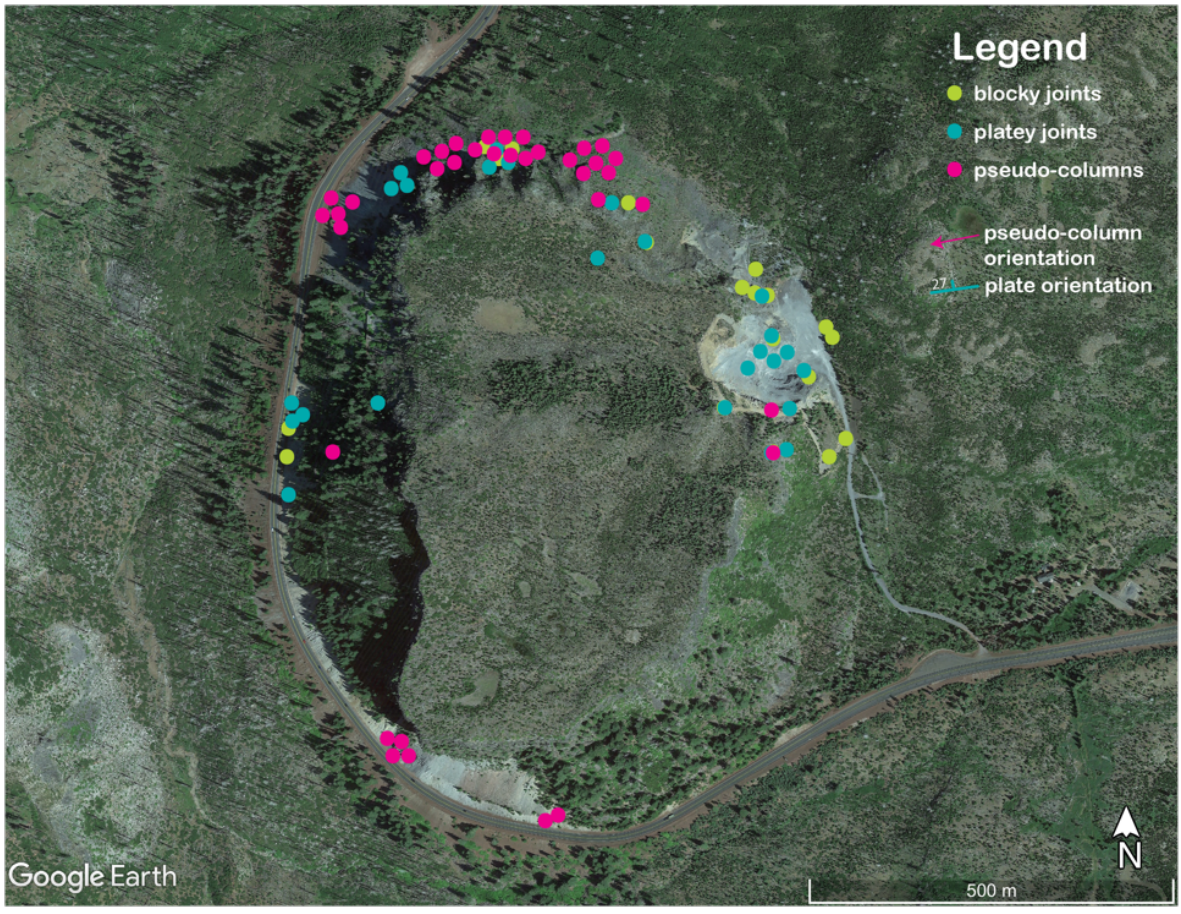

Figure 11: Locations of measured joints, color coded according to the type of joint. Green denotes blocky joints, blue denotes platey joints and pink denotes pseudo-columns. Note that the marked areas denote an observation of the joint, not necessarily a number density of orientation measurement.

Cube or "Blocky" Joints

The cube joints were the most prevalent of the three joint sets around the exposed outer faces of Hogg Rock. Cube jointing refers to more poorly-developed columnar jointing with blocky, irregular texture, which is thought to form by more coolant entering lava compared to when forming entablature (Forbes et al., 2014). The fractures bounding these blocks are too irregular to form coherent columns, suggesting either a faster or more irregular cooling history compared to more regular cooling columns. While some of these joints do form cube-shaped blocks with four bounding fractures, the blocks commonly have between three and six sides (Figure 12 and 13). These blocks vary in size between 0.1m and 1.25m, with an average width of 0.28m. The lava making up the blocks is very difficult to break with a hammer, and individual blocks are difficult to extract even along fractured surfaces. Typically, the cube joints have very poor

Figure 12: Cube joints at Hogg Rock, at outcrop scale (left) and at joint scale (right)


Figure 13: Schematic of how we measured joint density. For a given area (red box) we counted the blocks (cubes) present (white outlines)

exposure along the dimension of the fractures (in and out of the outcrop), but we note that where pseudo-columns are well exposed, cross-sections of the pseudo-columns appear very similar in style to the cube joints. Thus, it is also possible that these cube joints are simply a different orientation of columns, where instead of seeing the columns from the side (as you would in basalt columns such as those in Skinner Butte in Eugene), you are viewing them from the top or bottom, so that you cannot actually see a column structure. A notable way to identify glaciovolcanic features is by the chaotic orientation of cooling joints, and as such we cannot yet rule out the possibility of the cube joints in this case to be horizontally-oriented columnar joints.


Figure 14: Field camp students measuring cube joints.

In order to quantify the density of cube joints at Hogg Rock, we counted the number of cubes in a given square area at different locations around the butte. The measured area depended on the extent of the outcrop that was accessible. Figure 13 shows a schematic of how we counted the joints. For a horizontal and vertical length l_x and l_y, we counted the number of cubes n_x and n_y along those directions. Assuming a uniform density of blocks within a given outcrop, the number density of cube joints can be calculated as:

$$number\ density = \frac{n_x n_y}{l_x l_y}$$

Note that the goal of this measurement was to get a rough estimate for the number of joints (and joint density), and the assumption of uniform density is a simplification of the admittedly highly chaotic outcrops.

Note that the western side of Hogg Rock is mostly inaccessible on foot, so the majority of measurements for the number density were taken at outcrops on the eastern side of the butte and assumed to be representative of the other side. Observations noted from pullouts on the road at the western margin of Hogg Rock show that the western face of the butte is similar to the eastern side, with mainly blocky joints. The variety of l_x and l_y measured mainly due to how much of the exposure was accessible.

Platey Joints

Figure15: Large scale platey fractures in the gravel pit at Hogg Rock. Notice that all of the fracture sets have a preferred orientation, with those on the right having a subvertical preferred orientation, and a transition to blocky joints. (Bottom) Example measurement of platey fractures.

The platey joints were most notable within the "gravel pit" on the eastern side of Hogg Rock. These joints are highly fractured, and are characterized by thin, glassy plates bounded by very fine-density fractures. Unlike the blocky joints, these fractures have a clear preferred orientation within the scale of a given outcrop. However, the spacing and orientations of the platey joints appear to vary more significantly at greater lengths scales around the butte. In some areas, the boundaries between joints were sharp, others the boundary was curved. In addition, the surfaces of the platey fractures were often smooth or revealed plumose structures, which were harder to observe in the fractures with more chaotic surfaces such as the blocky joints. These structures indicate a clear direction of fracture propagation, which can be used to infer the

direction of cooling and thus potentially the direction of meltwater circulation that may have caused the rapid cooling.

For the platey fractures, we measured both the orientation (strike and dip) and average fracture spacing. To find the fracture spacing, we counted the number of fractures for a given length perpendicular to the orientation of the fractures, $\frac{n}{l}$, where n is the number of plates, and l is the perpendicular length measured.

Figure 16: Smaller scale platey fractures at Hogg Rock. Note that these sets also have a preferred orientation, but they occur between sets of other fractures.

In addition to these large-scale platey fractures primarily located in the gravel pit, there were also thinner, vertically extensive areas throughout Hogg Rock where the rock was more highly fractured in a platey fashion, creating smaller-scale platey fractures (Figure 16). While we did not conduct measurements for these, we did note them, as they may be indicative of a zone where more rapid cooling was occurring, leading to a more highly fractured section. In these areas, these fractures occur between other fracture sets, in what appears to be pre-existing fractures. It is not possible to determine if these small scale platey fractures occurred after the formation of the fractures on either side of it, or if these occurred simultaneously.

Figure 17: Pseudo-columnar joints at Hogg Rock. These columns are sub-horizontal, and appear blocky from a head on angle. Note the rectangular prism shape, which is not typical for columnar jointing. Image taken by Meredith Townsend

Pseudo-Columns

The last of the three sets of joints we identified were pseudo-columns. These refer to joints that appear columnar, but do not have the clean, sharp column shape you observe in places such as Skinner's Butte in Eugene. These also do not have the traditional polygonal shape, and are closer to cubic or rectangular prismatic columns. These fractures appeared to be the least common at Hogg Rock. These fractures were more prominent on the western side of the butte, however we were not able to quantify these due to the inaccessibility of that face. Additionally, the pseudo-columns had varying degrees of texture on them that oftentimes appeared similar to blocky joints, but they have surfaces that are longer in one dimension, making them appear more columnar. These textures include "bumpy" or rough textures, some columns were striated, and others had plumose structures. It is possible that the blocky joints and pseudo-columns are the same type of fracture, but appearing at different orientations with different amounts of three-dimensional exposure. In some areas, the boundaries between column sets were not linear, but had curving and gradual transitions to other joint sets (figure 18). For these fractures, we measured the trend and plunge of the columns, measuring the line of intersection of column-bounding faces. We also measured the number density of columns for a given length perpendicular to the columns, $\frac{n}{l}$, where n is the number of columns counted along a perpendicular length measured l.

Figure 18: Outcrop displaying a transition from finely spaced platey joints (lower) to pseudo-columnar joints (upper). This transition is gradual on the scale of tenths of meters. Image by Meredith Townsend.

CHAPTER IV: RESULTS

The results of our data collection are presented below. These have been split up into three sections. The first is a presentation of the petrology of Hogg Rock. The second is data pertaining to the number density of the fractures and their distribution across Hayrick Butte. A histogram summarizing the number density for all of the fractures is shown in figure 19. The third is data on the orientation of fractures, which pertains to measurements made on platey joints and pseudo-columns. These are discussed below.

Fracture Number Density

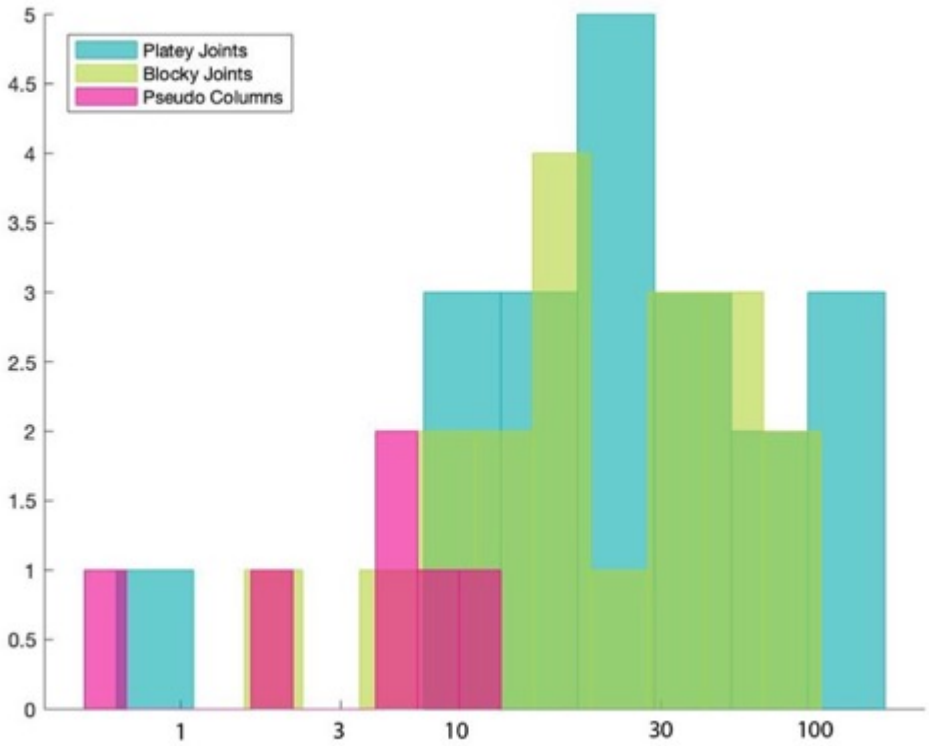

Figure 19: Histogram of the number density of fractures, with the x-axis representing the number density (in 1/m for platey joints and pseudo-columns, and $1/m^2$ for blocky joints), and the y-axis representing the number of outcrops in that number density. Note that the bin edges are different for each fracture type.

Blocky Joints

The blocky joints varied in width from 0.1 – 1.25m, with an average width of .28m. The density of the joints ranged from 1.6 – 85.5 m^{-2}, with an average number density of 28.6 m^{-2}. Most of the blocky joints (4 outcrops) had a joint density between 12.5 – 19 m^{-2}, and many (6 outcrops) were between 28 – 66 m^{-2}. Some outcrops had larger widths of blocky, and smaller joint densities (1.6 - 2.3 m^{-2}, 2.3 – 5.4 m^{-2}) as a result. A map of how these densities were distributed laterally across the butte is shown in Figure 20.

Platey Joints

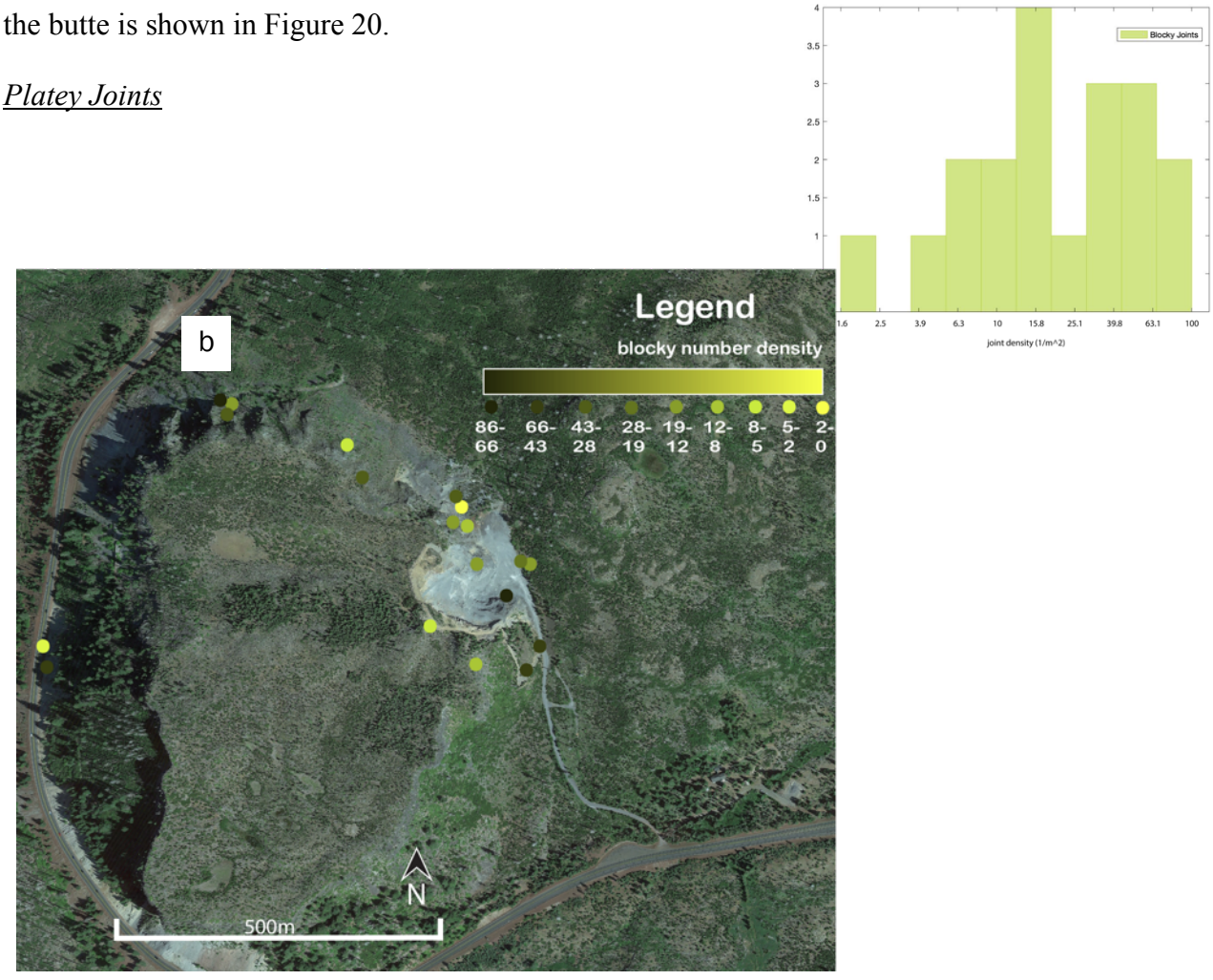

Figure 20: Lateral distribution of number density of blocky joints across Hogg Rock. A) Histogram showing the distribution of number densities, with x-axis representing the joint density ($1/m^2$), and y axis representing number of outcrops in a given bin. The bins edges are at 0 m^{-2}, 2.3 m^{-2}, 5.4 m^{-2}, 8.3 m^{-2}, 12.5 m^{-2}, 19 m^{-2}, 28 m^{-2}, 43 m^{-2}, 66m^{-2}, and 86 m^{-2}. B) Aerial image of Hogg Rock, with dots on areas where the joint density of blocky joints was measured. The colors of the dots correspond to the bins in the histogram. The lightest green represents the lower number density measurements, and dark greens represent highest number densities.

The density of the platey joints varied from 0.87m^{-1} – 128m^{-1}, with an average joint density of 36.5m^{-1} (Fig. 21a). Note that only one outcrop was at this lower range, with most outcrops having a number density higher than 5.75m^{-1}. Many outcrops (5) had a joint density between 17 – 30 m^{-1}, and most (14) were between 5.75 – 52.5 m^{-1}. A map of how these densities were laterally distributed throughout Hogg Rock is shown in figure 21.

a

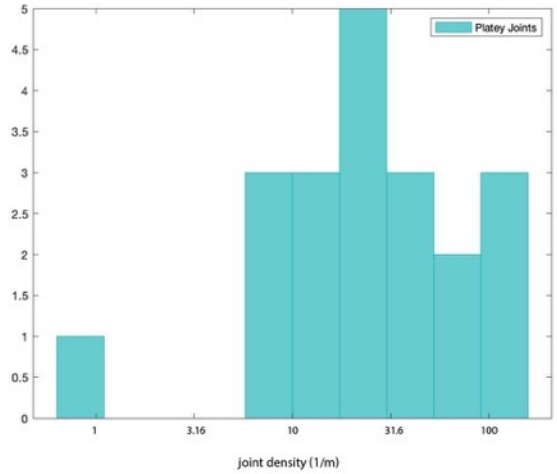

b

Figure 21: Lateral distribution of number density of platey joints across Hogg Rock. A) Histogram showing the distribution of number densities, with x-axis representing the joint density (1/m), and y axis representing number of outcrops in a given bin. The bins edges are at 0 m^{-1}, 5.75 m^{-1}, 10 m^{-1}, 17 m^{-1}, 30 m^{-1}, 52.5 m^{-1}, 91 m^{-1}, and 128 m^{-1}. B) Aerial image of Hogg Rock, with dots on areas where the joint density of platey joints was measured. The colors of the dots correspond to the bins in the histogram. The lightest blue represents the

Pseudo Columns

The pseudo-columns varied in width from 0.05 – 0.3m, with an average width of 0.175m (Fig 22a). Measurements for the number density of pseudo columns are sparse, with mainly three regions measured. In these areas, the number density varied from 0.53 – 10 m^{-1}, with an average number density of 4.83 m^{-1}. Note that only one area was in this lower range of number density, with most (4) measurements ranging from 3.9 – 1 m^{-1}. A map of how these measurements are laterally distributed across Hogg Rock is shown in Figure 22.

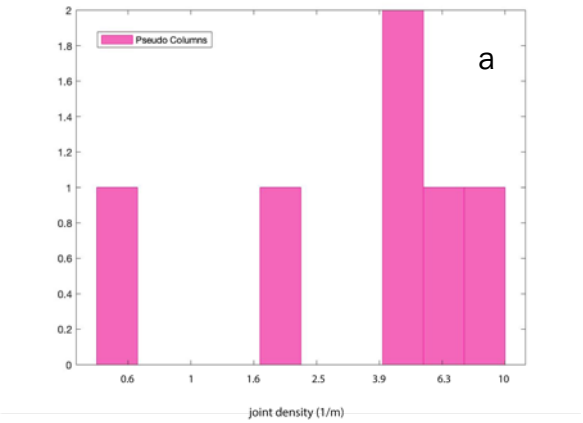

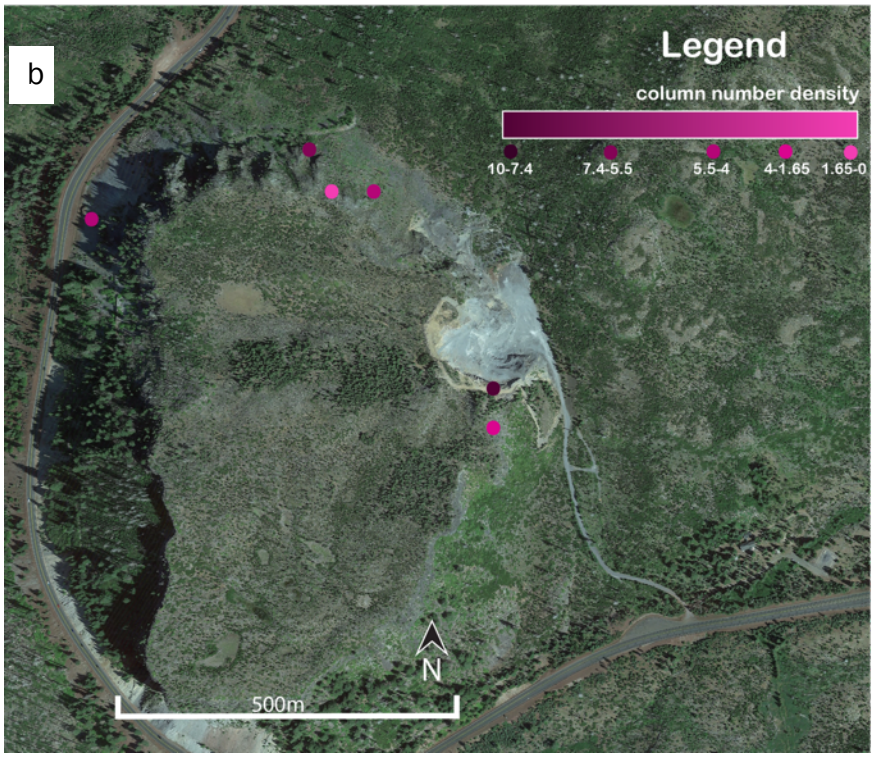

Figure 22: Lateral distribution of number density of pseudo columns across Hogg Rock. A) Histogram showing the distribution of number densities, with x-axis representing the joint density (1/m), and y axis representing number of outcrops in a given bin. The bins edges are at 0 m^{-1}, 1.65 m^{-1}, 3.9 m^{-1}, 5.5 m^{-1}, 7.4 m^{-1}, and 10 m^{-1}. B) Aerial image of Hogg Rock, with dots on areas where the joint density of pseudo columns was measured. The colors of the dots correspond to the bins in the histogram. The lightest pink represents the lower number density measurements, and dark pink represent highest number densities.

Fracture Orientation

For sets of fractures with a clear preferred orientation (occurring in the platey joints and the pseudo columns), we measured the orientation of numerous fractures and averaged them to obtain a map of the fracture orientations at Hogg Rock. The platey joints tended to be laterally extensive, with roughly the same orientation within each outcrop. For the pseudo-columns, we measured the trend and plunge of the line of intersection of column-bounding faces.

Platey Joints

A map for the average joint orientation and the lateral distribution of these across Hogg Rock is shown in figure 23. Note that the orientations presented are an average for each locality measured, with each representing an average of 2-3 measurements. The platey joints were primarily striking

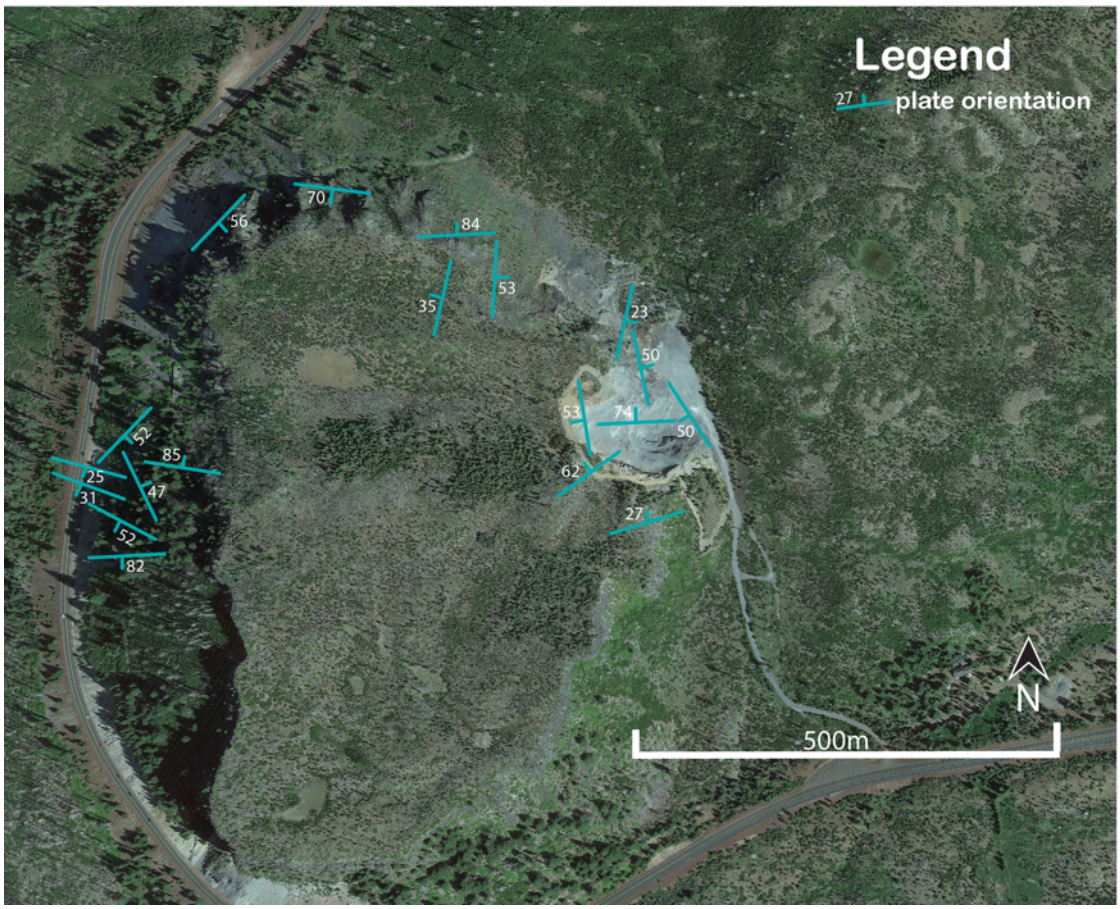

Figure 23: Aerial image of Hogg Rock, with the orientations of platey joints marked in blue, and the dip denoted with a white number. Dips are in degrees.

radially out from the butte, with some joints striking tangentially. The average dip of the plates was 55°.

Pseudo Columns

A map for the average joint orientation and the lateral distribution of these across Hogg Rock is shown in figure 24. Note that the orientations presented are an average for each locality measured, with each representing an average of 3-5 measurements. The pseudo columns primarily trended radially across the butte. The average plunge of the columns was 32°.

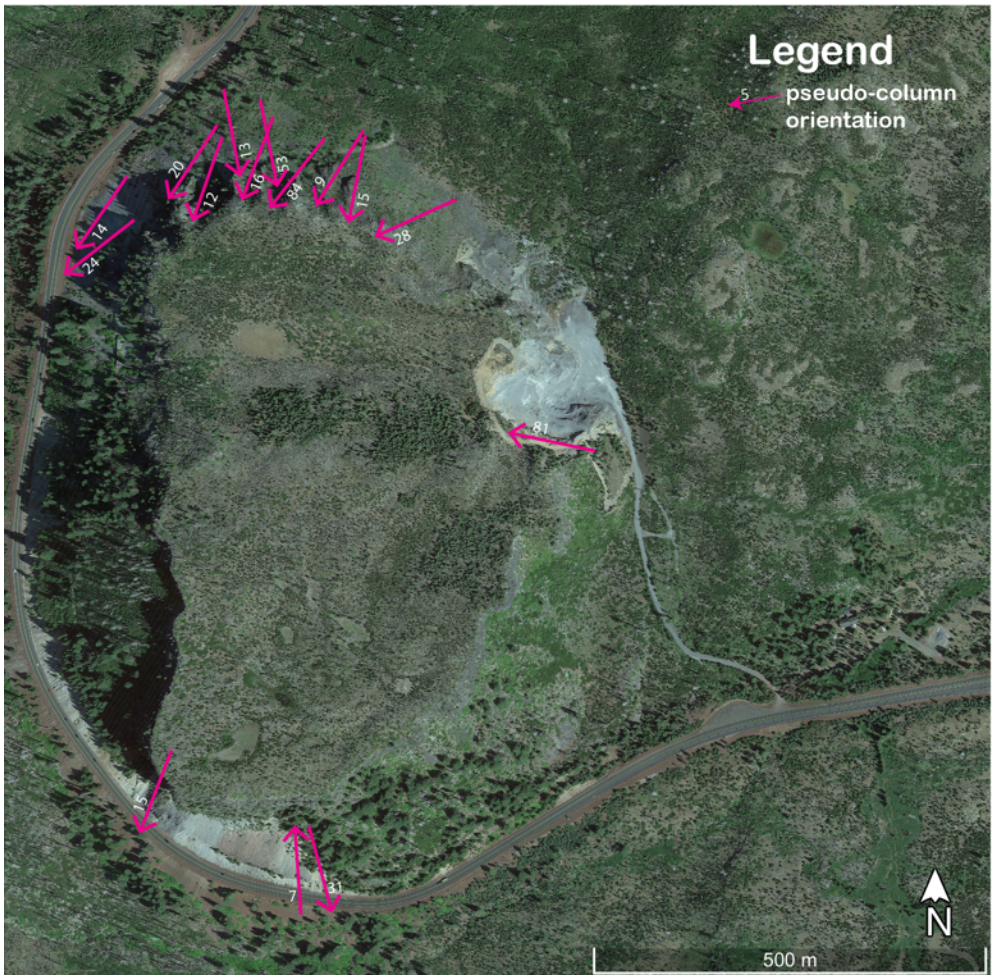

Figure 24: Aerial image of Hogg Rock, with the orientations of pseudo columns marked in pink, and the plunge denoted with a white number. Plunges are in degrees.

CHAPTER V: INTERPRETATION AND DISCUSSION

The style of cooling joints we observed is not entirely unique to Hogg Rock. Forbes et al. (2014) documented cooling joints they refer to as entablature in basaltic lava flows in Iceland. They hypothesized that these entablatures were formed where water was dammed by the lava flow and later breached the internal portion of the lava, suddenly enhancing the rate of cooling to form fine-density and chaotic fractures. The style of jointing in their entablature included cube-typed jointing like those we observed at Hogg Rock, where the lava flow is too irregularly fractured to observe any clear "column" feature. They also observed a style of entablature where the lava formed thin plates, however these features in their basaltic units were far more curved and chaotic than those we observed. In other words, their thinly jointed basalts did not exhibit a preferred orientation like those we recorded. In addition, they observed a style of pseudo columnar jointing that we observed at Hogg Rock, with main fracture systems forming columns that in themselves has differing textures that they inferred to be indicative of different cooling rates. The textures they noted in their pseudo-columns were far more regular, with striae on the surfaces of columns that were relatively equally spaced for each set of joints, and each joint set having different spacing in their columns. Textures within cooling columns can provide insight into the cooling history of the flow. At Hogg Rock, we were unable to identify many surface textures on the fracture except in the case of plumose structures within the platey joints. While they are not as direct of an indicator of cooling history as Forbes et al. predicted with their striae, plumose structures perhaps can be used to understand the directionality of fracture opening, and hence the direction of cooling surfaces. Future work to carefully examine plumose structures on cooling joint surfaces could add to our understanding of the source of cooling.

Another key difference between the joints we observed at Hogg Rock and other observed cooling joints is the shape of the columns. Phillips et al. (2013) studied columnar jointing in basaltic units in Scotland, with the goal of understanding how the column dimensions (i.e., the shape of the column) relate to the cooling history of the flow. They observed primarily 6-sided cooling columns. This is already significantly different from the columns we observed (both at Hogg Rock and at Hayrick Butte), which tended to be more rectangular prism-shaped rather than a hexagonal shape. Hexagonal columns are thought to represent slower and more regular cooling than columns with a lower hexagonality index. This is consistent with the interpretation that the columns at Hogg Rock formed more rapidly in response to an external coolant like glacial meltwater.

The orientation of fractures at Hogg Rock provides clues about the cooling history and potential interactions with ice. While there are some data gaps, the pseudo-columns display preferred orientations that appear to trend radially around the butte, with near-horizontal plunges. In general, it is understood that columns form in a direction that is perpendicular to the direction of cooling. Therefore, we believe that Hogg Rock was cooling from the outside in, with the cooling surfaces oriented vertically around the lava. This is consistent with the interpretation that Hogg Rock is a tuya and that the lava was in contact with a glacier on all sides when it erupted.

The different joint styles also indicate their relationship to different cooling conditions. For example, platey joints are significantly more densely fractured than blocky joints, which we interpret as an indication that the platey joints cooled more quickly than the blocky joints. The platey joints represent the finest scale of fracturing in our entire data set, which in turn suggests that the areas where platey joints are present represent the areas that cooled the most quickly at Hogg Rock. In addition, we qualitatively observed that the platey joints were glassier than the

other joint sets. The presence of this glassier texture suggests that the platey joints were quenched, likely by the presence of an external coolant when they were forming. We hypothesize that the platey joints formed after the initial contact with ice caused significant melting.

In addition, we do not see highly regular columns, which suggests that the cooling rates and cooling directions within these lavas were likely not as regular as typical subaerial lava flows. Cooling by meltwater circulation would likely produce more irregular cooling than ambient air flow in subaerial eruption. After initial contact between lava and ice creates meltwater, this water could then infiltrate the lava through the fractures, rapidly cooling and quenching the lava to produce even more fractures. The presence of smaller-scale secondary fractures stemming off of platey joints (figure 16) could have formed in this way.

Another clue about magma-meltwater interaction comes from the spatial relationship between the joint sets. The presence of the gravel pit at Hogg Rock provides a look into a deeper layer into the butte, which is also something we observed at Hayrick Butte in the form of a large lobe coming out from the cliff face. From this scoop into the buttes, it appears as if the blocky joints form an outer layer around the butte, with platey joints located further into the butte (this also supports the idea that the pseudo columns we observed are perhaps the blocky joints from a different perspective). The formation of outer blocky joints or pseudo columns would allow water to seep in and flash cool lava to form platey joints at different rates. This could also cause irregularity in the plate structures, causing more chaotic orientations due to variations in how much and how fast water seeped in and variations in water temperature.

We summarize a hypothesized series of events that explains the morphology and fracture pattern at Hogg Rock. Prior to eruption, the lavas were already very crystal rich as evidenced by flow textures in the plagioclase (Figure 8). The crystal content and higher silica content of the

andesite would lead to a relatively high-viscosity magma, which we would expect to erupt as a dome when no ice is present. The more table-shaped rather than dome-shaped morphology indicates the confinement by ice. As the magma came into contact with ice, the cooling rate would be enhanced, forming initial irregular fractures around the outside of the dome. However, the lower initial temperatures of andesitic lavas compared to basaltic lavas would lead to a slower cooling rate, which would explain the differences in the fractures we see at Hogg Rock compared to basaltic glaciovolcanic features. Over time, glacial meltwater would accumulate and create a layer between the ice and the magma, so that the main coolant is no longer the ice but is instead the meltwater. We hypothesize that the outer shell of Hogg Rock cooled quickly to form blocky joints/pseudo-columns, and then the meltwater was able to penetrate through the cooling fractures on the outer shell and into the interior of Hogg Rock, creating the layers of platey joints and other irregular fractures that we see. We expect the glacier above Hogg Rock was relatively thick, on the scale of hundreds of meters or at least as thick as Hogg Rock itself. If the glacier were any thinner than this, we would expect to see a passage zone and perhaps even explosive deposits. Thick glaciers may have allowed for the suppression of explosive activity.

The work presented here sets the groundwork for deciphering the cooling history at Hogg Rock, with primarily qualitative connections between the type of fracture and how this may relate to a difference in cooling rate. Future work should focus on quantifying these connections, in order to obtain a more precise measure for how the cooling rate of Hogg Rock varies spatially around the butte. One way to do this would be through sample analysis. We collected rock samples at different fracture sets at Hogg Rock. The first goal of this sample collected was to observe the crystals in thin section. Crystal Size Distribution (CSD) analysis can provide insight into the cooling history at Hogg Rock, as you would expect areas with larger crystals to have cooled more

slowly than those with smaller crystals. Another goal of the sample collection was to gain constraints on the emplacement history of Hogg Rock. By gathering oriented thin sections at Hogg Rock, we can look at the flow fabrics and gain an understanding of the direction of flow, and therefore gain some insight on whether Hogg Rock was an inflating dome or a stack of horizontal lava flows. Further flow fabric analysis can help to discern between these conceptual models.

We were also very limited in our fracture mapping due to the inaccessibility of many of the outcrops, particularly on the portion of Hogg Rock bordering HWY 20 and definitely at Hayrick Butte, another nearby tuya. In order to map these fractures in detail, we conducted drone surveys to create 3-D Structure from Motion (SfM) models of the buttes. Future work could continue the mapping of fracture sets for these two buttes on these SfM models, using a software like MetaShape or ArcGIS to create digital maps of the fractures. This would also allow for more measurements of the number density and widths of fractures to fill data gaps.

CHAPTER VI: CONCLUSION

Hogg Rock is a dome of intermediate composition located in the Oregon Cascades. Its flat top, steep sides, glacial striations and lakes at its top, and prevalent cooling fractures has led others to characterize it as a subglacial dome, or tuya. We mapped the cooling fractures at Hogg Rock and found three types of cooling joints: cube joints, which we interpret to be an outer shell that was in initial contact with the ice; platey joints, which we interpret to be an area of more rapid, chaotic cooling via an external coolant; and pseudo-columnar joints, which we interpret to be the blocky joints from a different orientation. We measured the fracture orientations for the pseudo-columns and platey joints, and found that the pseudo-columns are primarily horizontal and radially oriented around the butte, while the platey joints are more irregular. We interpret these data to mean that Hogg Rock cooled from the outside in, with a substantial component of cooling by water circulation through an outer layer of joints. This interpretation further supports the hypothesis that Hogg Rock was surrounded by a glacier during its eruption. Future work should focus on further constraining the cooling and emplacement history of Hogg Rock, in order to quantify the relationship between cooling rate and cooling fracture characteristics, and compare with other subglacial features in the area such as Hayrick Butte.

APPENDIX: HOGG ROCK FRACTURE DATA

Below is the raw data used for fracture density calculations and orientation mapping for this thesis. All data was collected by the University of Oregon Geology Field Camp in July of 2021. The colors correspond to the group that collected the data. Data sheet available upon request.

I. Cube Joints Spatial Data

Longitude (degrees)	Longitude	Altitude (ft)	Horizontal Length (m)	Number of Blocks	Vertical Length (m)	Number of Blocks	Label		density (joints/area)
44° 25' 27" N	-121° 52' 15" W	4820	1.6	4	1.6	4	b1		6.25
44 25 29.99	121 52 8.399	1463 (+/- 3) m	5.5	20	5.5	20	b2		13.2231405
44 25 29.99	121 52 12	1461 (+/- 3) m	4.44	21	6.94	21	b3		14.31186229
44 25 29.99	121 52 8.399	1463 (+/- 3) m	6.1	33	7	33	b4		25.50351288
44° 25' 25.4994"	121° 52' 7.7514"	1468	2	16	2	12	b5		48
44° 25' 24.7074"	121° 52' 8.58"	1477	4.9	37	2.5	18	b6		54.36734694
44º25'33"N	121º52'13"W	1520	2.5	2	1	2	b7		1.6
44º25'38"N	121º52'29"W	1410	2	8	1	3	b8		12
44º25'38"N	121º52'29"W	1420	2	12	1	3	b9		18
44º25'38"N	121º52'29"W	1420	2	19	1	9	b10		85.5
44º25'38"N	121º52'29"W	1420	2	12	1	6	b11		36
44° 25' 28.344"	121° 52' 9.912"	1467.073171	2	18	2	16	b12		72
44° 25' 24.7794"	121° 52' 42.096"	1367.682927	1.829	13	1.829	14	b13		54.40564671
44.42552° N	121.87017° W	1869	3	10	4	11	b14		9.166666667
44.42620°N	121.87217° W	1467	0.85	6	0.85	4	b15		33.21799308
44 25 32 N	121 52 13 W	4790 ft	3	18	3	15	b16		30
44 25 32 N	121 52 13 W	4790 ft	3.3	10	2.2	12	b17		16.52892562
44 25 36 N	121 52 21 W	4830 ft	2.75	10	2.75	6	b18		7.933884298
44 25 26 N	121 52 42 W	4490 ft	2.57	5	2	5	b19		4.86381323

II. Platey Joints Spatial and Orientation Data

Latitude (degrees)	Longitude (degrees)	Altitude	Length (m)	n	Strike (azimuth)	Dip		Number density (joints/m)
44° 25' 27" N	-121° 52' 15" W	4820	1.7	64	201	58		37.64705882
44° 25' 27" N	-121° 52' 11 " W	4820	n/a	n/a	229	48		
44° 25' 27" N	-121° 52' 11 " W	4820	2	37	272	80		18.5
44° 25' 29" N	-121° 52' 12" W	4820	1.3	33	281	76		25.38461538
44° 25' 29" N	-121° 52' 12	4820	n/a	n/a	262	71		
44° 25' 29" N	-121° 52' 12	4820	0.6	38	287	83		63.33333333
44° 25' 29" N	-121° 52' 12" W	4840	2.3	2	239	65		0.869565217
44 25 29.99	121 52 12	1470 (+/- 5)	1.62	15	348	50		9.259259259
44° 25' 33.6"	121° 52' 22.8714"	1463	6.5	67	193	35		10.30769231
44° 25' 27.156"	121° 51' 36.504"	1492	2.5	119	279	85		47.6
44º25'25"N	121º52'12" W	1525	1	63	214	28		63
44º25'25"N	121º52'12" W	1525	1	101	272	26		101
44º25'25"N	121º52'12"W	1525	1	11	275	26		11
44° 25' 28.7034"	121° 52' 13.5474"	1492.07317	1	128	S05E	51W		128
44° 25' 28.7034"	121° 52' 13.5474"	1492.07317	n/a	n/a	S13E	55W		
44° 25' 28.596"	121° 52' 10.056"	1472.56098	0.5	46	S33E	50W		92
44° 25' 26.5434"	121° 52' 41.628"	1367.68293	0.609	10	N70w	31W		16.42036125
44° 25' 26.3994"	121° 52' 41.772"	1367.37805	0.914	6	N62W	52W		6.564551422
44° 25' 26.3994"	121° 52' 41.772"	1367.37805			N87E	82E		
44° 25' 26.3994"	121° 52' 41.772"	1367.37805			N44E	52E		
44° 25' 26.3994"	121° 52' 41.772"	1367.37805			N26W	47E		
44° 25' 31.8714"	121° 52' 12.612"	1869	2	35	12.5	22.5		17.5
44° 25' 34.32"	121° 52' 19.8114"	1467	0.85	5	3	53		5.882352941
44° 25' 36" N	121° 52' 22" W	4800	0.9	33	S82W	84		36.66666667
44 25 23 N	121 52 42 W	4520 ft	1.65	30				18.18181818
44 25 27 N	121 52 42 W	4490 ft	1.55	33	S75E	25		21.29032258
44° 25' 36.5592"	121° 52' 35.6844"	8.85318534			140.6262665	52.0276032		
44° 25' 36.5838"	121° 52' 35.5224"	8.69851938			130.1183014	54.1641121		
44° 25' 36.5442"	121° 52' 35.5542"	4.03984906			130.3950806	59.3688469		
44° 25' 37.6212"	121° 52' 28.8588"	16.2132395			190.9350128	72.026886		
44° 25' 37.4988"	121° 52' 29.1864"	5.23021714			184.7451477	72.6598434		
44° 25' 37.4988"	121° 52' 29.1864"	5.23021714			184.1219788	66.1602783		

III. Pseudo-Columns Spatial and Orientation Data

Latitude	Longitude	Altitude	Length Measured (m)	Number of columns	Number density	Trend	Plunge
44° 25' 36.084"	121° 52' 22.8714"	1487	13	7	0.538461538		
44° 25' 26.832"	121° 52' 12.0714"	1462	4.7	47	10		
44º25'25"N	121º52'12"W	1525	2	4	2		
44° 25' 37.4154"	121° 52' 23.6994"	1443					
44° 25' 38.172"	121° 52' 29.892"	1408	1.8	13	7.222222222	193	55
						197	39
						212	44
44° 25' 38.28"	121° 52' 28.776"	1417				193	55
						197	39
						212	44
44° 25' 37.884"	121° 52' 26.7234"	1431				223	83
						220	85
						212	84
44° 25' 35.148"	121° 52' 39.3234"	1346					
44° 25' 24.7794"	121° 52' 39.3234"	1365					
44° 25' 11.5674"	121° 52' 35.4354"	1396					
44 25 36 N	121 52 20 W	4810 ft	4.5	20	4.444444444	259	28
44 25 35 N	121 52 39 W	4450 ft	4.8	23	4.791666667	232	24
44° 25' 8.778"	121° 52' 25.9278"					165.6947937	31.55932808
44° 25' 8.8134"	121° 52' 25.9962"					356.2901001	6.96016073
44° 25' 11.5782"	121° 52' 35.187"					199.4813995	15.60222912
44° 25' 11.7048"	121° 52' 35.4318"					188.3825684	20.62560272
44° 25' 11.6502"	121° 52' 35.349"					215.4851532	7.15800905
44° 25' 35.4648"	121° 52' 39.507"					257.2546692	25.93570137
44.42649763	-121.8776474					110.444397	1.06419408
44.42654684	-121.8777555					277.0393066	15.30354023
44.42718557	-121.875945					214.4094086	18.40124321
44.42709531	-121.8759257					212.5119324	21.84147835
44.42720525	-121.8755269					190.1468353	4.57415152
44.42720785	-121.8756256					212.0417786	18.53553772
44.42722504	-121.8747986					149.0148926	16.26612282
44.42722596	-121.8748813					179.2020569	12.38876057
44.42718246	-121.8748594					181.580719	11.47993755
44.42740859	-121.8746595					202.1719666	18.89740944
44.42734533	-121.8746461					196.4715424	12.86075783
44.42729064	-121.8749564					174.1332703	51.13513565
44.42732248	-121.8749619					166.1732941	55.04246521
44.42711715	-121.8731833					198.3367462	9.52409458
44.42713237	-121.8731588					218.3849182	1.59139991
44.42715092	-121.8731452					220.5636597	15.08996868
44.42719693	-121.8732963					209.2916412	4.36347151
44.42719643	-121.8735026					182.4371033	14.62585163
44.42720768	-121.8734979					182.1642914	27.26863289

REFERENCES CITED

Allen, C. C., Jercinovic, M. J., & Allen, J. S. B. (1982). Subglacial Volcanism in North-Central British Columbia and Iceland. *The Journal of Geology*, *90*(6), 699–715. https://doi.org/10.1086/628725

B., E., J., R., & R., A. (2002). Subglacial, phonolitic volcanism at Hoodoo Mountain volcano, northern Canadian Cordillera. *Bulletin of Volcanology*, *64*(3–4), 254–272. https://doi.org/10.1007/s00445-002-0202-9

Báez, A. D., Báez, W., Caselli, A. T., Martini, M. A., & Sommer, C. A. (2020). The glaciovolcanic evolution of the Copahue volcano, Andean Southern Volcanic Zone, Argentina-Chile. *Journal of Volcanology and Geothermal Research*, *396*, 106866. https://doi.org/10.1016/j.jvolgeores.2020.106866

Bleick, H. A., Coombs, M. L., Cervelli, P. F., Bull, K. F., & Wessels, R. L. (2013). Volcano–ice interactions precursory to the 2009 eruption of Redoubt Volcano, Alaska. *Journal of Volcanology and Geothermal Research*, *259*, 373–388. https://doi.org/10.1016/j.jvolgeores.2012.10.008

Deligne, Natalia I., Mckay, Daniele, Conrey, Richard M, Grant, Gordon R., Johnson, Emily R., O'Connor, Jim, & Sweeney, Kristin. (2017). *Field-trip guide to mafic volcanism of the Cascade Range in Central Oregon—A volcanic, tectonic, hydrologic, and geomorphic journey* (Scientific Investigations Report).

Edwards, B. R., Russell, J. K., & Simpson, K. (2011). Volcanology and petrology of Mathews Tuya, northern British Columbia, Canada: glaciovolcanic constraints on interpretations of the 0.730 Ma Cordilleran paleoclimate. *Bulletin of Volcanology*, *73*(5), 479–496. https://doi.org/10.1007/s00445-010-0418-z

Edwards, B. R., Gudmundsson, M. T., & Russell, J. K. (2015). Chapter 20 - Glaciovolcanism. In H. Sigurdsson (Ed.), *The Encyclopedia of Volcanoes (Second Edition)* (pp. 377–393). Amsterdam: Academic Press. https://doi.org/10.1016/B978-0-12-385938-9.00020-1

Evatt, G. W., & Fowler, A. C. (2007). Cauldron subsidence and sub-glacial floods. *Annals of Glaciology*, *45*, 163–168.

Farquharson, J. I., James, M. R., & Tuffen, H. (2015). Examining rhyolite lava flow dynamics through photo-based 3D reconstructions of the 2011–2012 lava flowfield at Cordón-Caulle, Chile. *Journal of Volcanology and Geothermal Research*, *304*, 336–348. https://doi.org/10.1016/j.jvolgeores.2015.09.004

Forbes, A. E. S., Blake, S., & Tuffen, H. (2014). Entablature: fracture types and mechanisms. *Bulletin of Volcanology*, *76*(5), 820. https://doi.org/10.1007/s00445-014-0820-z

Gudmundsson, M. T., Pálsson, F., Björnsson, H., & Högnadóttir, $\mathcal{H}$. (2002). The hyaloclastite ridge formed in the subglacial 1996 eruption in Gjálp, Vatnajökull, Iceland: present day shape and future preservation. *Geological Society, London, Special Publications*, *202*(1), 319–335. https://doi.org/10.1144/GSL.SP.2002.202.01.16

Gudmundsson, Magnús T. (2003). Melting of ice by magma-ice-water interactions during subglacial eruptions as an indicator of heat transfer in subaqueous eruptions. In J. D. L. White, J. L. Smellie, & D. A. Clague (Eds.), *Geophysical Monograph Series* (Vol. 140, pp. 61–72). Washington, D. C.: American Geophysical Union. https://doi.org/10.1029/140GM04

Gudmundsson, Magnús T., Sigmundsson, F., Björnsson, H., & Högnadóttir, T. (2004). The 1996 eruption at Gjálp, Vatnajökull ice cap, Iceland: efficiency of heat transfer, ice deformation and subglacial water pressure. *Bulletin of Volcanology*, *66*(1), 46–65. https://doi.org/10.1007/s00445-003-0295-9

Hildreth, W. (2007). *Quaternary magmatism in the Cascades: geologic perspectives*. Reston, Va: US Dept. of the Interior, US Geological Survey.

Hill, B. E. (1992). *Geology and geothermal resources of the Santiam Pass area of the Oregon Cascade Range, Deschutes, Jefferson and Linn Counties, Oregon* (No. DOE/ID/12834-13; USGS-OFR-0-92-3). Oregon State Dept. of Geology and Mineral Industries, Portland, OR (United States). https://doi.org/10.2172/7018867

Jouzel, J., Lorius, C., Petit, J. R., Genthon, C., Barkov, N. I., Kotlyakov, V. M., & Petrov, V. M. (1987). Vostok ice core: a continuous isotope temperature record over the last climatic cycle (160,000 years). *Nature*, *329*(6138), 403–408. https://doi.org/10.1038/329403a0

Lachowycz, S. M., Pyle, D. M., Gilbert, J. S., Mather, T. A., Mee, K., Naranjo, J. A., & Hobbs, L. K. (2015). Glaciovolcanism at Volcán Sollipulli, southern Chile: Lithofacies analysis and interpretation. *Journal of Volcanology and Geothermal Research*, *303*, 59–78. https://doi.org/10.1016/j.jvolgeores.2015.06.021

Lodge, R. W. D., & Lescinsky, D. T. (2009). Fracture patterns at lava–ice contacts on Kokostick Butte, OR, and Mazama Ridge, Mount Rainier, WA: Implications for flow emplacement and cooling histories. *Journal of Volcanology and Geothermal Research*, *185*(4), 298–310. https://doi.org/10.1016/j.jvolgeores.2008.10.010

McGarvie, D. (2009). Rhyolitic volcano–ice interactions in Iceland. *Journal of Volcanology and Geothermal Research*, *185*(4), 367–389. https://doi.org/10.1016/j.jvolgeores.2008.11.019

Oddsson, B., Gudmundsson, M. T., Edwards, B. R., Thordarson, T., Magnússon, E., & Sigurðsson, G. (2016). Subglacial lava propagation, ice melting and heat transfer during emplacement of an intermediate lava flow in the 2010 Eyjafjallajökull eruption. *Bulletin of Volcanology*, *78*(7), 48. https://doi.org/10.1007/s00445-016-1041-4

Phillips, J. C., Humphreys, M. C. S., Daniels, K. A., Brown, R. J., & Witham, F. (2013). The formation of columnar joints produced by cooling in basalt at Staffa, Scotland. *Bulletin of Volcanology*, *75*(6), 715. https://doi.org/10.1007/s00445-013-0715-4

Reynolds, H. I., Gudmundsson, M. T., Högnadóttir, T., Magnússon, E., & Pálsson, F. (2017). Subglacial volcanic activity above a lateral dyke path during the 2014–2015 Bárdarbunga-Holuhraun rifting episode, Iceland. *Bulletin of Volcanology*, *79*(6), 38. https://doi.org/10.1007/s00445-017-1122-z

Russell, J. K., Edwards, B. R., Porritt, L., & Ryane, C. (2014). Tuyas: a descriptive genetic classification. *Quaternary Science Reviews*, *87*, 70–81. https://doi.org/10.1016/j.quascirev.2014.01.001

Sherrod, D. R., & Smith, J. G. (1990). Quaternary extrusion rates of the Cascade Range, northwestern United States and southern British Columbia. *Journal of Geophysical Research*, *95*(B12), 19465. https://doi.org/10.1029/JB095iB12p19465

Smellie, J. L., & Edwards, B. R. (2016). *Glaciovolcanism on Earth and Mars: products, processes, and palaeoenvironmental significance*. Cambridge: Cambridge University Press.

Stevenson, J. A., Gilbert, J. S., McGarvie, D. W., & Smellie, J. L. (2011). Explosive rhyolite tuya formation: classic examples from Kerlingarfjöll, Iceland. *Quaternary Science Reviews*, *30*(1), 192–209. https://doi.org/10.1016/j.quascirev.2010.10.011

Tuffen, H., & Castro, J. M. (2009). The emplacement of an obsidian dyke through thin ice: Hrafntinnuhryggur, Krafla Iceland. *Journal of Volcanology and Geothermal Research*, *185*(4), 352–366. https://doi.org/10.1016/j.jvolgeores.2008.10.021

Wilson, L., & Head, J. W. (2007). Heat transfer in volcano–ice interactions on Earth. *Annals of Glaciology*, *45*, 83–86. https://doi.org/10.3189/172756407782282507